J Mater Sci: Mater Med (2015) 26:260
DOI 10.1007/s10856-015-5586-0

BIOCOMPATIBILITY STUDIES

Original Research

Protein, cell and bacterial response to atmospheric pressure plasma grafted hyaluronic acid on poly(methylmethacrylate)

Raechelle A. D'Sa[1,2] · Jog Raj[2] · Peter J. Dickinson[2] · M. Ann S. McMahon[3] · David A. McDowell[3] · Brian J. Meenan[2]

Received: 3 June 2015 / Accepted: 25 September 2015 / Published online: 8 October 2015

Abstract Hyaluronic acid (HA) has been immobilised on poly(methyl methacrylate) (PMMA) surfaces using a novel dielectric barrier discharge (DBD) plasma process for the purposes of repelling protein, cellular and bacterial adhesion in the context of improving the performance of ophthalmic devices. Grafting was achieved by the following steps: (1) treatment of the PMMA with a DBD plasma operating at atmospheric pressure, (2) amine functionalisation of the activated polymer surface by exposure to a 3-aminopropyltrimethoxysilane (APTMS) linker molecule and (3) reaction of HA with the surface bound amine. The mechanism and effectiveness of the grafting process was verified by surface analysis. XPS data indicates that the APTMS linker molecule binds to PMMA via the Si–O chemistry and has the required pendant amine moiety. The carboxylic acid moiety on HA then binds with this $-NH_2$ group via standard carbodiimide chemistry. ToF-SIMS confirms the presence of a coherent HA layer the microstructure of which is verified by AFM. The plasma grafted HA coating surfaces showed a pronounced decrease in protein and cellular adhesion when tested with bovine serum albumin and human corneal epithelial cells, respectively. The ability of these coatings to resist bacterial adhesion was established using *Staphylococcus aureus* NTC8325. Interestingly, the coatings did not repel bacterial adhesion, indicating that the mechanism of adhesion of bacterial cells is different to that for the surface interactions of mammalian cells. It is proposed that this difference is a consequence of the specific HA conformation that occurs under the conditions employed here. Hence, it is apparent that the microstructure/architecture of the HA coatings is an important factor in fabricating surfaces intended to repel proteins, mammalian and bacterial cells.

✉ Raechelle A. D'Sa
r.dsa@liverpool.ac.uk

[1] Centre for Materials and Structures, University of Liverpool, Brownlow Hill, Liverpool L69 3GH, UK

[2] Nanotechnology and Integrated Bio-Engineering Centre (NIBEC), University of Ulster, Shore Road, Newtownabbey BT37 0QB, UK

[3] Biomedical Sciences Research Institute, School of Heath Sciences, University of Ulster, Shore Road, Newtownabbey BT37 0QB, UK

1 Introduction

Non-specific adsorption or "biofouling" of biological molecules on synthetic surfaces is a heavily researched area as it can significant consequences on the successful implantation of a wide range of devices. Additionally, adhesion of these biomaterial surfaces with bacteria can also result in the failure or rejection of the device. Hence, there is a technological requirement for several medical devices to have antifouling surfaces; particularly for ophthalmic applications. For example, an optically transparent cornea, essential for normal visual function needs to be replaced by an artificial cornea (keratoprosthesis) if opacification due to disease or injury occurs. Opacification can lead to monocular blindness and hence keratoprosthesis have been fabricated from a wide variety of transparent materials, including poly(methyl methacrylate) (PMMA), poly(2-hydroxyethyl methacrylate) (p-HEMA) and hydrogels [1–3]. PMMA was the first polymer used for the construction of keratoprosthesis due to its inherent bioinert properties and although it is less common in the latest generation of implant devices, it is still seen as an excellent model for assessing bioresponse [4, 5]. However, the

hydrophobic nature of PMMA can result in the non-specific adsorption or fouling by biological components, particularly proteins [6] that subsequently result in negative biological reactions [7–9].

Several strategies have been investigated to add biofunctionality to PMMA by modifying its surface properties and controlling the subsequent biological response [6, 10, 11]. Previous studies by the authors have demonstrated that grafting of hydrophilic polymers such as poly(ethylene glycol) (PEG) onto polymeric biomaterials via a plasma processing methodology operating at atmospheric pressure, is an effective way of modifying their surface chemistry and modulating the biological response in terms of protein adsorption and cellular adhesion [10, 12]. However, PEG can be oxidised in vivo; therefore, modification using alternative more robust hydrophilic polymers is an attractive alternative. To this end, we have shown previously that hyaluronic acid (HA) can be successfully grafted onto a polystyrene (PS) surface using plasma assisted grafting [10]. This study illustrates PMMA surfaces modified with HA as a way to control protein, cell and bacterial adhesion in the context of enhancing biomaterials for applications such as keratoprosthesis function.

HA is a naturally occurring macromolecule belonging to the glycosaminoglycan (GAG) family and is present in extracellular matrix, vitreous humor, synovial fluid and cartilage [13, 14]. It is a high molecular weight linear polymer made up of the glucoronic acid (1-β-3) *N*-acetyl-glucosamine (1-β-4) disaccharide repeating unit. In solution, HA has a coiled structure that is highly hydrated with a 200 nm radius of gyration. This highly hydrated structure has roughly 1000-fold more water than the native polymer [15]. HA is negatively charged at pH 7.4 and its viscosity allows it to behave like a polyelectrolyte, i.e. to dissociate in aqueous solution. It is these hydrodynamic properties of HA that are responsible for its role in extracellular matrix and other tissues [16]. The ability of HA to promote water retention has rendered it ideally suited to ophthalmic biomaterial applications. As such, HA has been used widely for eye drop solutions [17, 18] and as a viscoelastic fluid to alleviate intraocular pressure during intraocular surgeries [19].

The clinical use of HA is limited, however, by its poor mechanical properties. Several studies have shown the immobilisation of HA onto polymer surfaces, via both physical and chemical methodologies, allows for the fabrication of surfaces with increased biocompatibility [20–24]. Many of the protocols used to create a HA adlayer employ complicated synthetic pathways that need lengthy optimisation and therefore are limited for scale up applications. Hence, there remains an ongoing need for versatile immobilisation strategies that are capable of inducing robust covalent tethering of HA onto a medically relevant biomaterials. Furthermore, an understanding of how these HA-coated surfaces behave in a biological environment needs to be elucidated as the conformation of the grafted polymer is known to affect its subsequent interaction with proteins and cells.

In this study we report a novel method for the preparation of HA modified PMMA surfaces using atmospheric pressure plasma processing. The technique is based on that used previously to immobilize PEG on PMMA [25]. However, in this case, once PMMA has been oxidatively functionalized by exposure to the plasma, chemisorption of an aminosilane linker molecule (3-aminopropyl)trimethoxysilane (APTMS)) is introduced. The pendant amino group from the linker is then used for the subsequent tethering of HA via carbodiimide chemistry. The grafting mechanism has been verified by surface analysis (XPS and ToF-SIMS) while the resulting changes in surface morphology are determined by AFM. The behaviour of these HA modified surfaces with respect to protein adsorption and both mammalian and bacterial cellular adhesion is reported.

2 Materials and methods

2.1 Materials

Commercial grade PMMA (1.1 mm thick) sheets (Goodfellow, Cambridge UK) were used as the polymer substrate for these studies. Sheets were cut into 1.5 cm × 1.5 cm sized squares for convenient chemical and topographical analysis. For the protein and cell culture studies, 34 mm diameter discs were punched from the polymer sheet. In the case of the immunofluorescence staining studies 22 mm diameter discs were employed to facilitate imaging. Samples were cleaned by sonication in ethanol for 15 min and dried in air overnight prior to use. HA, as the sodium salt derived from *Streptococcus equi* (Fluka, UK) was used as received. In respect of the linker chemistry, water-soluble 1-ethyl-3(3-dimethylaminopropyl)carbodiimide hydrochloride (EDC, Fluka, UK), *N*-hydroxy succinimide (NHS, Sigma-Aldrich), (3-aminopropyl)trimethoxysilane (APTMS, Sigma-Aldrich, UK), and 2-(*N*-morpholino)ethane sulfonic acid (MES) were all used as received.

2.2 Atmospheric pressure plasma treatment

Plasma surface treatment was carried out at atmospheric pressure via exposure to a highly controlled dielectric barrier discharge (DBD) regime. The operational characteristics of the DBD reactor (Arcotec GmbH, Mönsheim, Germany) have been described in detail elsewhere [26–29]. In brief, the polymer samples were placed on a moving platen that constitutes the ground electrode which then

passes under a set of three metal wire working electrodes giving rise to a micro-streamer type electrical discharge condition. In this way, the polymer was treated at an energy dose (D) of 105 J/cm^2 corresponding to a power density (P_d) of 5.3 W and residence time of 18.8 s in the plasma (R). All experiments were carried out at a platen transit speed through the plasma region of 0.48 m/s.

2.3 Immobilisation of hyaluronic acid onto PMMA

HA was grafted onto PMMA using the reaction pathway illustrated in Fig. 1. The native polymer surface was DBD treated in air at atmospheric pressure, silanised, and subsequently grafted by carbodiimide mediated coupling. Step-by-step procedures for each stage of the process are provided below:

2.3.1 Silanisation of PMMA

Following the DBD treatment of PMMA, samples were immersed in a solution of 10 % w/w solution of (3-aminopropyl)trimethoxysilane (APTMS, Sigma-Aldrich, UK) in methanol for 60 s. The silanised samples were washed with methanol and dried in an oven at 50 °C for 2 h.

2.3.2 Chemical grafting of hyaluronic acid with EDC

HA was dissolved in a solution of 0.01 M MES buffer at a concentration of 3 mg/cm^3. The carboxylic acid group of the HA molecule was activated by adding NHS and EDC sequentially to make up a final concentration of 0.2 M EDC and 0.05 M NHS. The solution was stirred for 1 h at room temperature after which the silanised PMMA samples were immersed in the activated HA and incubated at room temperature overnight on a rocker table. The samples were then washed with Milli-Q ultrapure water for 24 h and dried at ambient temperature and pressure after which they were stored in sterile Petri dishes prior to analysis.

2.4 XPS analysis

X-ray photoelectron spectroscopy (XPS) was carried out using a Kratos Axis Ultra DLD spectrometer (Kratos, UK)

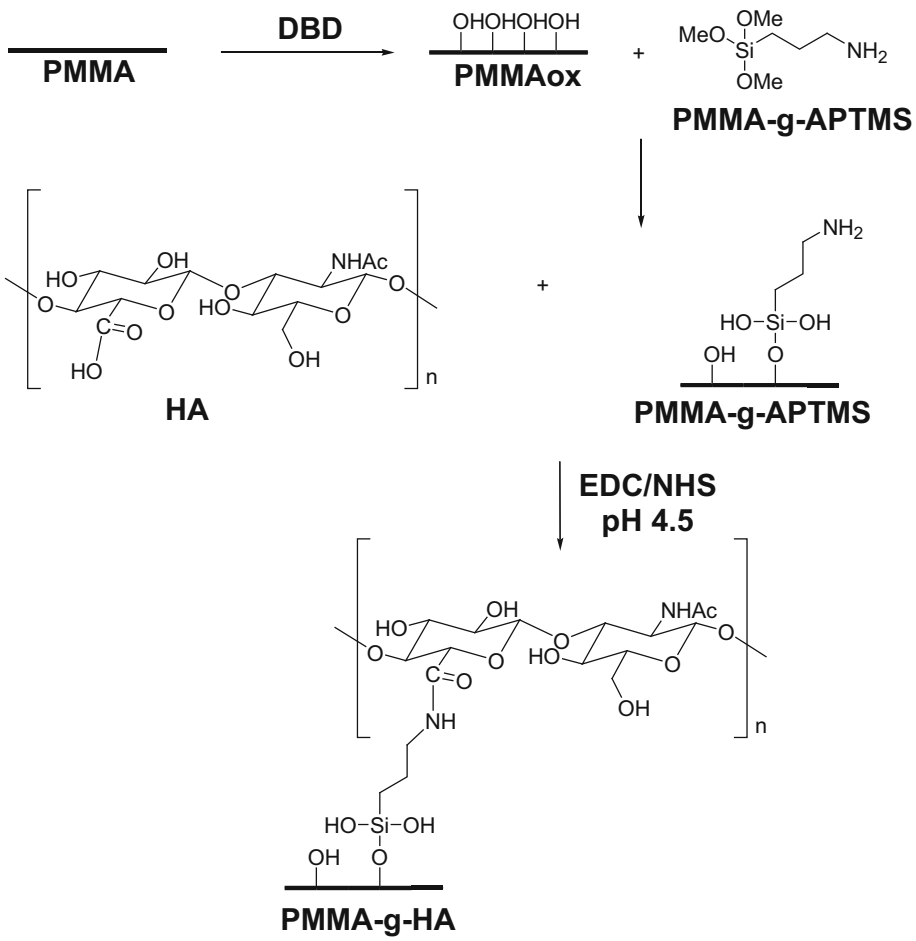

Fig. 1 Reaction scheme of the atmospheric pressure DBD plasma assisted immobilisation of HA on to PMMA

with a typical pressure during analysis of $<5 \times 10^{-8}$ Torr. A monochromated AlKα X-ray (1486.6 eV) source operating at an anode voltage of 15 kV and a 10 mA current was used throughout. Neutralisation of the effects of charging on the insulating polymer surfaces during analysis was provided using a low energy electron source working in tandem with the instruments magnetic immersion lens. As necessary, binding energy (BE) positions were further charge corrected by setting the most intense C1s component to 285.0 eV [30]. A "slot" aperture was used to attain spectra from area of analysis of 700 μm in the x-direction and 300 μm in the y-direction. Wide energy survey scans (1–1300 eV) were recorded at a pass energy 160 eV and corresponding high resolution spectra at 20 eV. Quantitative analysis was obtained for three individual areas of each sample with data reported as relative atomic % concentration (% At. conc.) Data manipulation was carried out using CasaXPS software (Version 2.3.15, Casa software, UK) with subtraction of a linear background and peak area measurement for the most intense spectral lines for all the elements detected. Spectra were curve fitted after the linear background subtraction using a mixed Gaussian–Lorentzian (70:30) function. All data are reported as average values ±1 standard deviation.

2.5 ToF-SIMS analysis

Time-of-flight secondary ion mass spectrometry (ToF-SIMS) measurements were performed using a ToF-SIMS V (ION-TOF GmbH, Germany) instrument. A bismuth liquid metal ion gun (LMIG) generating Bi_3^{2+} cluster ions was used as the primary ion source operating with the reflectron analyser and microchannel plate detector using a post-acceleration setting of 20 kV. The primary ion dose density for all analyses was kept within static SIMS limit (i.e. $<10^{12}$ cm^{-2}). Spectral acquisition and image analysis were carried out using IonSpec Version 4.1.0.1 and IonImage Version 3.1.0.14 software, respectively (ION-TOF GmbH, Germany). Pulses of low energy electrons from a flood gun were applied to samples between periods of secondary ion collection to compensate for charging effects on the insulating polymer surfaces. Mass resolved secondary ion images were recorded with the Bi_3^{2+} cluster ion source in burst alignment mode. Three replicate false colour images in the positive mode were recorded for each sample type.

2.6 AFM analysis

AFM was used to compare the topographical changes that occurred during the HA grafting process. A digital instruments (DI) NanoScope SPM (Vecco Metrology Group, USA) operating under ambient conditions was used. Images were acquired in tapping mode with a silicon tip mounted on a cantilever with a spring constant of 40 Nm^{-1} operating at a resonant frequency of 300 kHz and scan rate 1 Hz. Samples were imaged over a 1.0 μm × 1.0 μm sample area at a resolution of 512 × 512 pixels and using NanoScope 6.11r1 software (Vecco Metrology Group, USA). Zero-order plane fitting was used to remove any image distortion that results from the scanner moving out of plane with the sample. Elimination of errors in piezo linearity was corrected for by zero and first order flattening. Both mean surface roughness (R_a) and root mean square roughness (R_q) values were calculated from three replicates of each sample type.

2.7 Protein response

Protein response to the various samples was carried out using previously described methods [25]. Specifically, a 1 mg/cm^3 (w/v) solution of bovine serum albumin (BSA) produced from fatty acid and globulin-free lyophilised powder (Sigma-Aldrich, U.K.) was prepared in a 0.1 M phosphate buffered saline (PBS) solution. Samples were exposed to 3.0 cm^3 of this protein solution for 1 h. (this time period has been shown to be sufficient to allow for maximum adsorption, as previously seen by quartz crystal microbalance with dissipation analysis studies) [6]. Samples were then immersed in Milli-Q water and placed on a shaker for 15 min and then rinsed three times with Milli-Q water and allowed to dry overnight at room temperature. The various surfaces were then analysed by XPS and ToF-SIMS to elucidate whether or not any of the proteinaceous components had been adsorbed.

2.8 Mammalian cell response

Samples were sterilised by placing them in 70 % aqueous ethanol for 1 h and leaving them to dry in a laminar flow hood. A freshly prepared stock solution of 0.6 % Agar (Sigma-Aldrich, UK) in Milli-Q water was autoclaved at 123 °C for 15 min. Molten Agar (200 μL) was pipetted into sterile six-well plates and the polymer samples carefully placed on top such only the top surface of the sample is exposed.

Immortalised human corneal epithelial cells (hCECs) were used to assess the response of air DBD processed surfaces in cell culture. This hCECs cell line, was established by Dr. K. Araki-Sasaki (Kagoshima, Japan) by infecting hCECs with a recombinant SV40-adenovirus vector in 1995 [31]. The required number of cells for the studies undertaken here were cultured in a humidified atmosphere in Dulbecco's minimum essential medium

(DMEM, Gibco, UK) with F12 HAM nutrient mix supplemented with 10 % fetal bovine serum (FBS, Sigma, UK), 100 IU/mL penicillin G, 100 μg/mL streptomycin sulfate, and 20 μg/mL gentamycin (all obtained from Invitrogen, UK) under standard cell culture conditions of humidified atmosphere at 37 °C, 5 % CO_2. The cells were maintained below 70 % confluence and passaged every three to four days using 0.05 % trypsin–EDTA (Sigma, UK) into 75 cm^3 (Nunc, UK) tissue culture flasks.

The hCEC cells were seeded onto the various sample surfaces at a concentration of 2×10^5 cells/cm^2 and cultured under normal humidified conditions at 37 °C, 5 % CO_2. Cell media was changed every 2 days. All subsequent assays were carried out in triplicate and repeated three times to confirm results.

2.8.1 Cell counts

At each sampling time point the media was aspirated and the cells were washed twice with PBS (Gibco, UK) and morphologically fixed using 10 % paraformaldehyde (PFA, Sigma-Aldrich, UK). After 15 min, the samples were washed with PBS (3×2 cm^3) and exposed to 2 cm^3 of a 1:4 methanol:PBS solution for 15 min. To count the number of cells on each surface at each time point, samples were transferred to new well plates washed with PBS at 37 °C (3×2 cm^3) and permeabilised using 4 % PFA with 0.1 % Triton X-100 in PBS for 20 min. The samples were again washed with PBS (3×2 cm^3 for 5 min) to remove any traces of PFA. The samples were rinsed in PBS (3×5 min) and mounted on glass slides with Vectashield Mounting Medium containing 1.5 μg/cm^3 of 4′-6-diamidino-2-phenylindole (DAPI) counterstain (Vector Laboratories, UK). The slides were imaged using an epifluorescence microscope (Nikon Eclipse 80*i*). The number of cells was determined as the average of five measurements from each of three replicates of each surface type.

2.8.2 MTT cell viability assay

A stock solution of 5 mg/cm^3 MTT [3-(4,5-dimethylthiaol-2-yl)-2,5-diphenyltetrazolium bromide] (Sigma-Aldrich, UK) was prepared in PBS, passed through a 0.2 mm filter and stored at 4 °C. Cells were cultured on the various substrates as indicated in the previous section. After 24 and 48 h, the culture media was replaced with 2 cm^3 of phenol-free DMEM media (Gibco, UK) containing MTT at a concentration of 500 μg/cm^3. The cells were incubated at 37 °C in a humidified 5 % CO_2 atmosphere until the formazan product was visible ($\sim$1.45 h). The culture medium was aspirated off and the cells solubilised using a 0.1 M HCl in propanol solution. A 350 μL aliquot of the solvent was added to each well and after 10 min on a gyro-rocker aliquots of 100 μL pertaining to each sample type were transferred in triplicate to a 96-well plate, giving a total of nine replicates per sample type. Absorbance (optical density) was read in a Tecan SunriseTM (TECAN GmbH, Austria) microplate reader equipped with Magellan Software using a 570 nm filter.

2.9 Bacterial cell response

Bacterial cell response studies were carried out using previously reported protocols [32]. A Gram-positive bacterium *Staphylococcus aureus* NTC8325 was pre-cultured in Luria–Bertani (LB) broth (5.0 g of sodium chloride, 5.0 g of Tryptone, 2.5 g of yeast extract in 500 cm^3 of distilled water) at 37 °C. The optical density of the culture was adjusted to 0.1 at 600 nm. HA grafted PMMA samples that, in this instance, were treated on both sides of the substrate were placed in sterile 12 well plates and 2 cm^3 of bacterial cell suspension added into each well. The samples were incubated at 37 °C for 30 min and adhesion was allowed to take place on both sides. Gently rinsing three times with PBS was used to eliminate the non-adherent bacteria and the samples transferred to universals containing 10 cm^3 sterile PBS and sonicated for 10 min. After sonication, samples were plated onto agar plates and incubated at 37 °C overnight. The bacterial response was determined by plotting the number of colony forming units versus the experimental conditions. All samples were run in triplicate and repeated three times. As a control experiment, to measure whether any components of the broth adhered onto the samples, the samples were placed in sterile 12 well plates with 2 cm^3 of LB broth for 30 min at 37 °C. After 30 min, the surfaces were rinsed with PBS, and then water to remove any buffer salts that could interfere with the analysis. These surfaces were analysed by XPS and ToF-SIMS to elucidate whether any of the proteinaceous components had adsorbed.

2.10 Statistical analysis

Statistical analysis of the data obtained for all of the surface analysis and biological assays was performed with Origin® (v. 7.0383, OriginLab Corporation, USA). One way analysis of variance (ANOVA) was used to compare mean values in order to determine equivalence of variance between pairs of samples. Significance between groups was determined using the Bonferroni multiple comparison test. A value of $P < 0.05$ was taken as statistically significant. Results are reported as means ± standard deviation. Unless otherwise indicated, all experiments were carried out in triplicate and repeated twice.

3 Results

3.1 Modification of PMMA grafting of HA

As indicated earlier, the HA grafted surfaces were prepared by a three step process: DBD plasma treatment, self-assembly of an aminosilane layer and covalent attachment of HA. The DBD plasma, operating in air at atmospheric pressure, creates reactive species that bombard the PMMA surface leading to chemical (oxidation) and physical (etching) modification [6, 25]. Specifically, oxidative species are created on PMMA via the generation of plasma induced surface bound radicals which can then react with other (free) oxygen radicals generated by the plasma discharge to form peroxy, hydroperoxide and hydroxyl function groups on the polymer surface. In step two, the hydroxyl and/or hydroperoxide groups initiate self-assembly of the APTMS layer on PMMA to give an aminated surface. The final step involves tethering of the HA to the amide bond via carbodiimde/NHS chemistry.

3.1.1 Surface chemistry: XPS

Quantitative XPS data reporting the percentage atomic concentration (% At. conc.) of the elements detected at each stage of the grafting process are given in Table 1. The corresponding C1s high resolution spectra are shown in Fig. 2 with the relative contributions of each of the component peaks fitted to the experimental spectral envelope provided in Table 2. These data indicate that the DBD treatment of PMMA induces only a subtle change in the oxidation of the surface as shown by negligible difference in the % At. conc. values post processing. However, the high resolution C1s data (Fig. 2; Table 2), confirms that DBD treatment results in a decrease in the alkyl components (C–C/C–H) with a simultaneous rise in the C–O and O=C–O components, confirming that slight oxidation of the PMMA surface does occur.

The second step in the reaction pathway involves the amination of the DBD activated PMMA surfaces and this effect is confirmed with introduction of the N1s and Si2p peaks in the XPS spectra (Fig. 2). The experimental % At. conc. values for the APTMS linker layer are consistent with the theoretical values (Tables 1, 2). The discrepancy for the high resolution is the values in Table 2 is deemed to be due to the XPS sampling depth being larger than the thickness of the aminosilane layer. The orientation of the aminosilane on the PMMAox surface can be deduced by peak fitting of the corresponding N1s peak (Fig. 3a). It has been shown previously that the nitrogen from the APTMS can exist in up to three states [21, 33–38]. The XPS data indicates that the nitrogen moiety exists here in three states: protonated (401.5 eV), hydrogen-bonded (400.4 eV) and free amine (399.3 eV) [21]. The dominance of the contribution at 399.3 eV confirms that the APTMS binds to the oxidised PMMA surface via the silane functionality leaving pendant amine groups.

The third step in the reaction scheme was the binding of HA onto the aminated PMMA surface. The corresponding high resolution C1s data (Table 2) shows an increase in contributions from functionalities: C–N/C–O (286.3–286.5 eV) and C=O/O=C–N (288.0 eV). These results are in agreement with previously reported XPS data for HA [21, 39, 40]. The grafting of the HA is further confirmed by analysis of the N1s which shows a decrease in the amount of protonated amine (401.5 eV), and an increase in the amide peak (399.5 eV) contribution signifying that a bond has formed between the pendant amino group on the APTMS surface and the carboxylic acid on the HA. Once again the slight discrepancy between experimental (XPS) in and theoretical values is assumed to be due to the sampling depth ($\sim$5–10 nm) for the chemically bound HA layer being larger than in the case of the "dry" state molecular structure.

3.1.2 Surface chemistry: ToF-SIMS

Positive ion ToF-SIMS imaging was carried out to determine the lateral uniformity of the coatings on a 100 μm^2 scale. Figure 4 confirms the homogeneity of the chemical changes that are induced by each step in the reaction pathway. The secondary ions detected at 59 ($C_3H_7O^+$) and 69 ($C_4H_5O^+$) amu in the corresponding SIMS spectra have been used to characterise changes in PMMA (Fig. 4a) and PMMAox (Fig. 4b). As noted previously, exposure to the plasma environment causes only subtle changes to the

Table 1 XPS derived % At. conc. values for each stage of the processing leading to immobilisation of HA on PMMA

Substrate	O1s	N1s	C1s	Si2p
PMMA	27.3 ± 0.3		72.7 ± 0.3	
PMMAox	27.9 ± 0.4		72.1 ± 0.4	
PMMA-g-APTMS	23.2 ± 0.04	9.8 ± 0.4	57.6 ± 0.7	9.3 ± 0.3
PMMA-g-HA	15.1 ± 1.2	16.7 ± 0.1	67.5 ± 1.0	0.7 ± 0.1
Theoretical APTMS	27.3	9.1	54.5	9.1
Theoretical HA	42.3	3.8	42.3	0.0

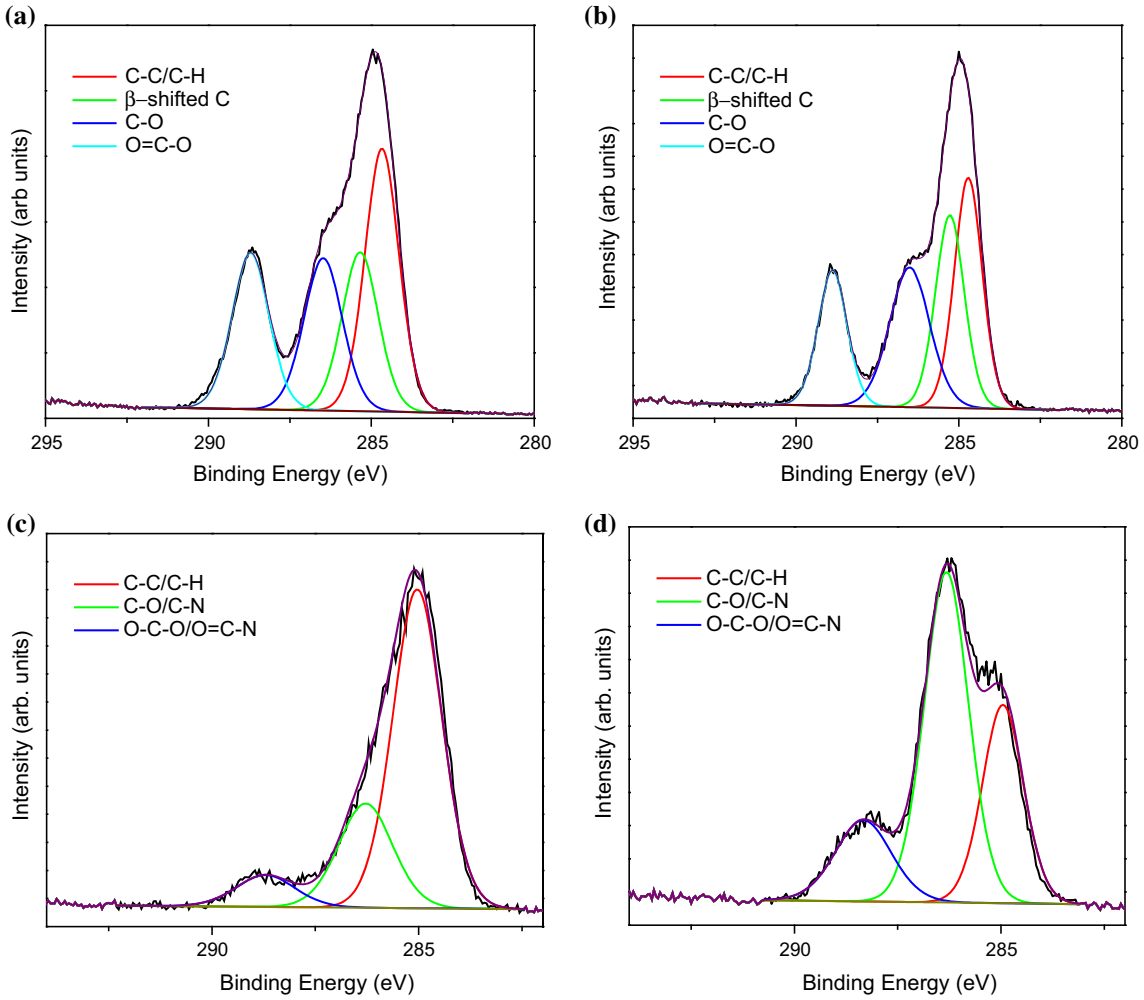

Fig. 2 Curve fitted C1s XPS spectra for **a** PMMA, **b** PMMAox and **c** PMMA-g-APTMS, **d** PMMA-g-HA surfaces

Table 2 XPS derived % At. conc. values for the contributions to the deconvoluted C1s spectral envelope for each stage of the processing leading to immobilisation of HA on PMMA

Substrate	C–C/C–H	C–O/C–N[a]	O=C–N/O=C–O
PMMA	57.6 ± 0.8	22.1 ± 1.3	20.3 ± 2.1
PMMAox	47.5 ± 3.3	30.0 ± 1.8	22.5 ± 5.1
PMMA-g-APTMS	69.1 ± 3	23.3 ± 2.9	7.6 ± 0.1
PMMA-g-HA	32.0 ± 2.1	50.1 ± 4.5	18.3 ± 2.1
Theoretical APTMS	40	60	0
Theoretical HA	7.1	64.3	28.6

[a] C–N is only present in PMMA-g-APTMS, PMMA-g-HA, theoretical APTMS, and theoretical HA samples

PMMA surface chemistry. Grafting of the APTMS and HA layers was confirmed by observing mass fragments at *m/z* 30, 41 and 58 amu indicative of CH_4N^+, $C_2H_3N^+$ and $C_3H_8N^+$, respectively. A significant decrease in the intensity of the characteristic PMMA peaks (m/z 59 and 69 amu) confirms the self-assembly of the APTMS layer (Fig. 4c). As peaks associated with mass fragments from PMMA are still visible in Fig. 4c, this indicates that the APTMS layer is thinner than ToF-SIMS sampling depth of 2–3 nm. After the HA immobilisation stage, the contributions from the (PMMA) peaks at m/z 59 and 69 are negligible, thereby indicating that the combined APTMS and HA layers on the polymer are now greater than of 2–3 nm ToF-SIMS sampling depth. Hence, when considered with the corresponding XPS analysis, these collective data indicate that the thickness of the APTMS/HA layer is less than sampling depth of XPS (~5–10 nm) but greater than the sampling depth of ToF-SIMS (2–3 nm).

3.1.3 Surface morphology: AFM

AFM was used to study the morphological changes that occurred during the HA grafting process with the

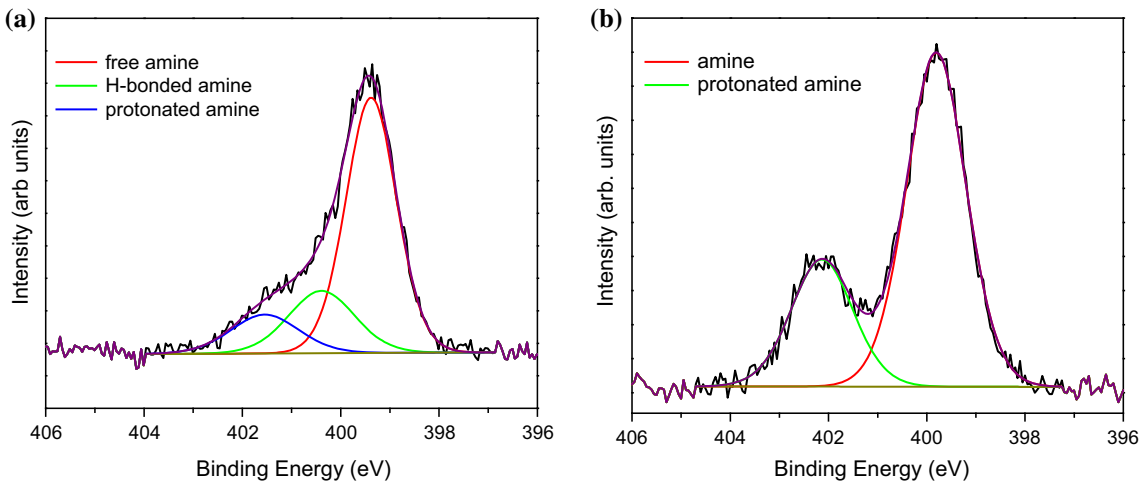

Fig. 3 Curve fitted N1s XPS spectra for **a** PMMA-g-APTMS, **b** PMMA-g-HA surfaces

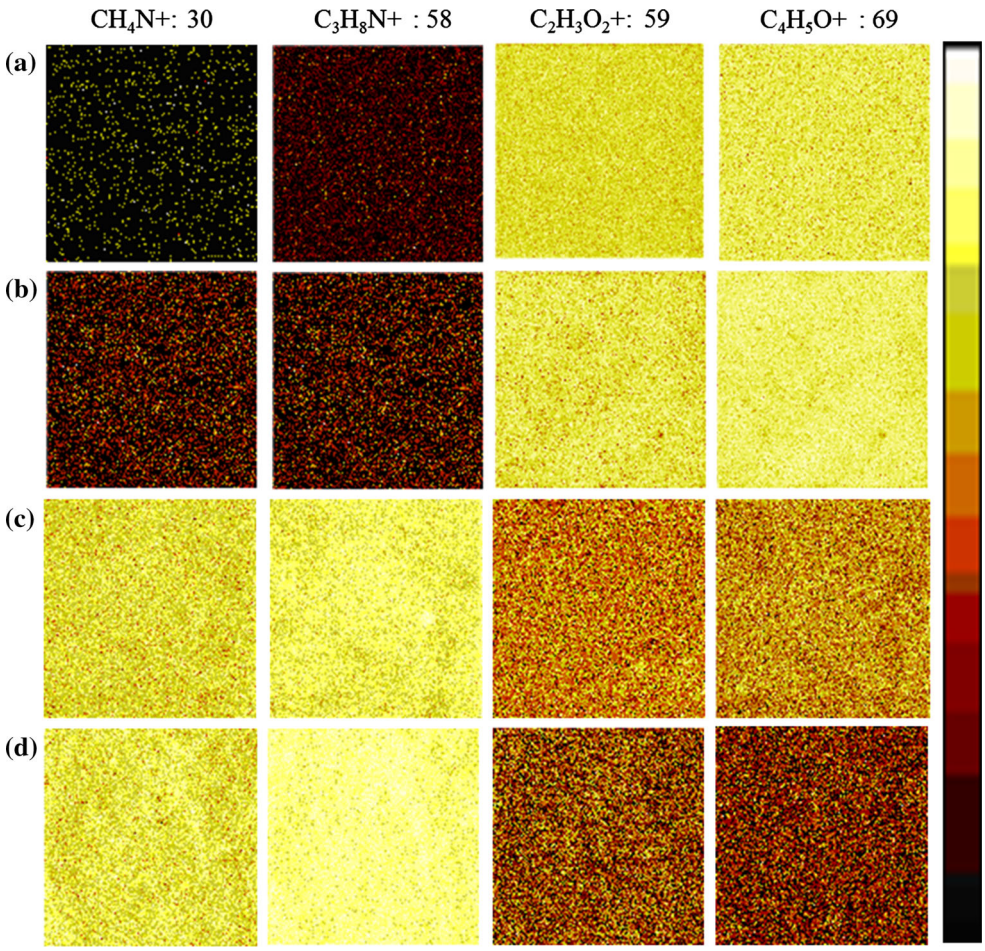

Fig. 4 ToF-SIMS images (100 μm × 100 μm) created from the positive ion counts detected at m/z 30, 59, and 69 amu for **a** pristine PMMA, **b** PMMAox, **c** PMMA-g-APTMS, **d** PMMA-g-HA surfaces (intensity scale shows increasing ion counts from dark to light coloured areas)

respective images and surface roughness values given in Fig. 5. Pristine PMMA has an average surface roughness value (R_a) of 0.7 ± 0.0 nm which increases slightly to 2.5 ± 0.1 nm after DBD treatment. This is deemed to be a result of chain scission of the PMMA polymer chains caused by DBD plasma induced etching of the polymer surface. As such, the PMMAox image indicates a regular distribution of spherical features at the scale indicated. Self-assembly of the APTMS linker layer causes a noticeable smoothening of the PMMAox surface

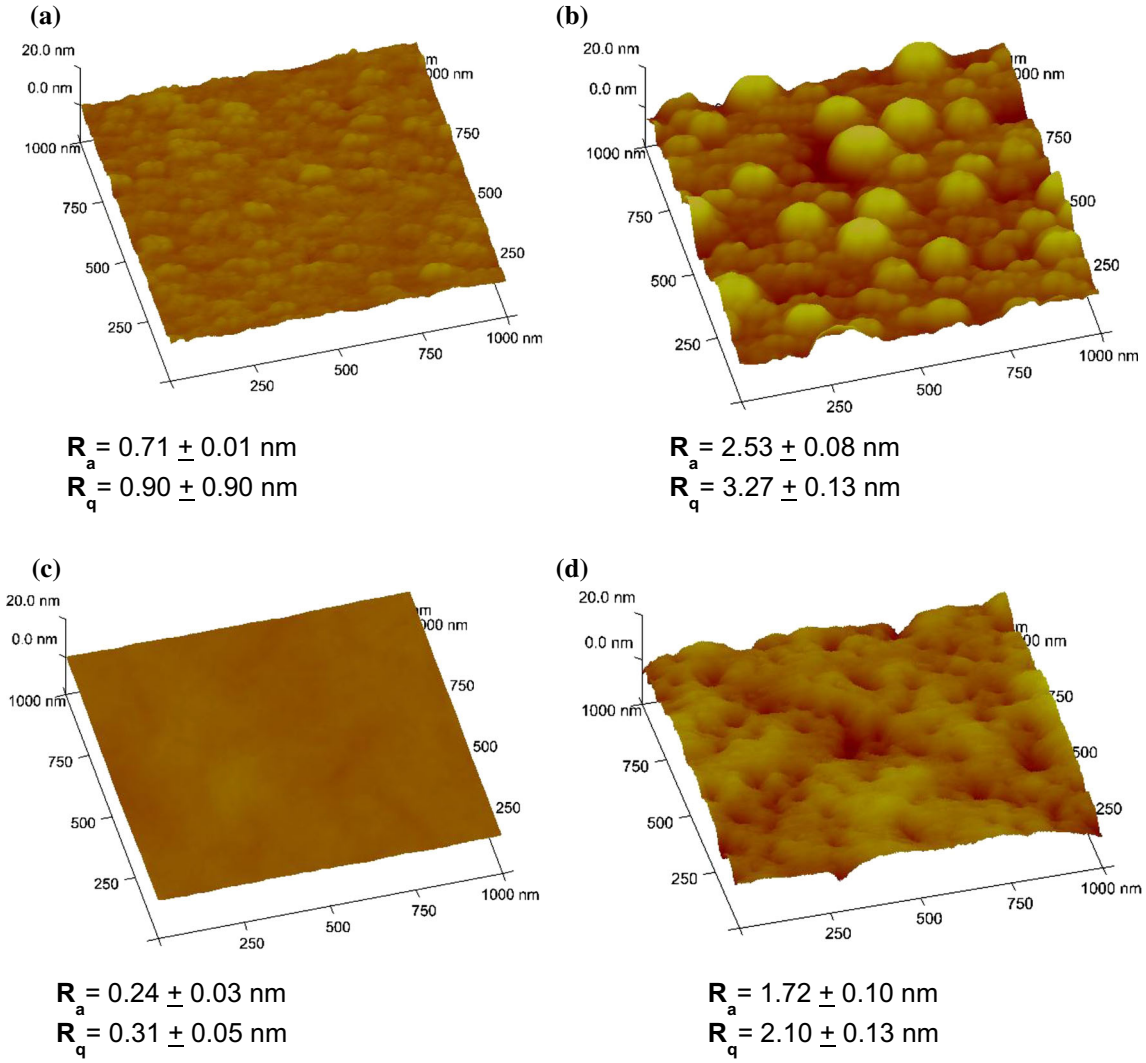

Fig. 5 AFM images for **a** PMMA, **b** PMMAox, **c** PMMA-g-APTMS, **d** PMMA-g-HA surfaces

($R_a = 0.2 \pm 0.0$ nm), indicating that the chemisorbed APTMS has a conformation which masks the topography of the underlying PMMAox surface. The PMMA-g-HA surface has a R_a value of 1.7 ± 0.1 nm and the AFM image which indicates that HA has a more ordered structure APTMS layer. Overall, these data corroborate the interpretation of the ToF-SIMS images and confirm the homogeneity of each of the grafting steps.

3.2 Biological evaluation of variously modified PMMA surfaces

3.2.1 Protein response

XPS analysis of the PMMA-g-HA surfaces exposed to BSA (data not shown) showed no increase in the N1s signal suggesting that the surfaces are capable of rejecting protein adsorption, at least in regard to the detection limit of the technique. The positive ion ToF-SIMS spectra for a PMMA-g-HA surface after BSA adsorption is given in Fig. 6 and indicates the presence of amino acid fragments (Ala, Pro, Val, Lys, Ile, Leu, His, Phe and Trp) thereby suggesting that some protein adsorption has taken place. Hence, this PMMA-g-HA surface is not capable of rejecting protein adsorption at the detection limit of ToF-SIMS.

3.2.2 Mammalian cell response

Cell counts of hCECs on PMMA, PMMAox, PMMA-g-APTMS and PMMA-g-HA surfaces were monitored 1, 3 and 7 days after seeding with the data presented in Fig. 7. The PMMAox and PMMA-g-APTMS surfaces had a statistically significantly increase in adherent cells compared

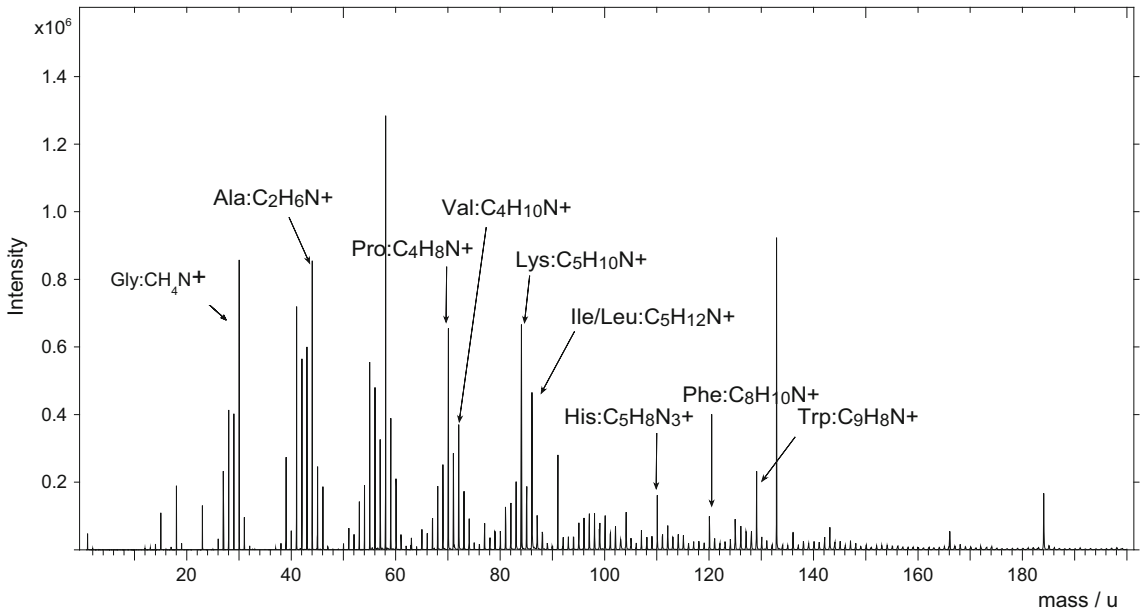

Fig. 6 Positive ion ToF-SIMS spectrum for PMMA-g-HA surface after incubation with BSA for 30 min

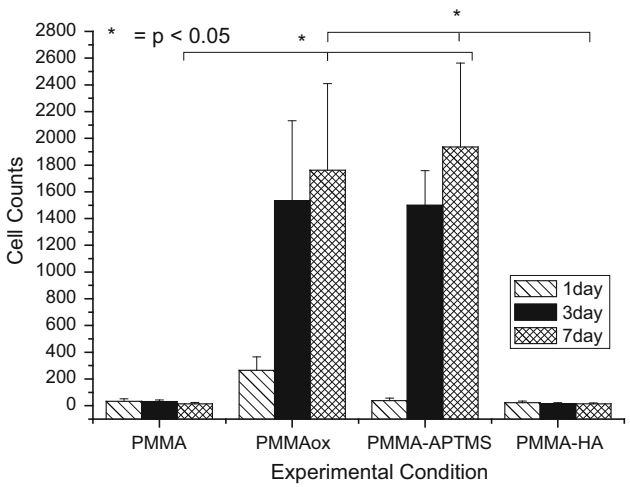

Fig. 7 Cell counts for human corneal epithelial cells (hCECs) on the variously modified PMMA samples 1, 3 and 7 days post seeding

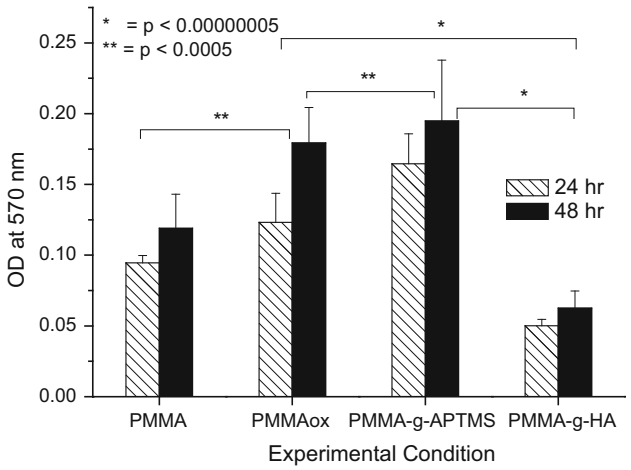

Fig. 8 MTT assay data for activity of human corneal epithelial cells (hCECs) on the various PMMA samples 24 and 48 h post seeding

to pristine PMMA and PMMA-g-HA. Indeed, these results indicate that the PMMA-g-HA surface was successful in completely knocking out hCEC adhesion at all of the time points (1, 3 and 7 days) studied.

Data for hCEC viability, as analysed via an MTT assay at 24 and 48 h post seeding is shown in Fig. 8. As was the case for the cell counts studies, there was a statistically significantly ($P < 0.000005$) greater number of viable cells on the PMMAox and PMMA-g-APTMS surfaces compared to the pristine PMMA and PMMA-g-HA surfaces. Hence, the HA immobilised surface was successful in repelling both cell adhesion and proliferation.

3.2.3 *Bacterial cell response*

The ability of the surfaces of interest to prevent bacterial adhesion was studied by incubation with *S. aureus* NTC-8325 for 30 min with the resulting data shown in Fig. 9. The number of bacteria adhering to the HA modified surface (PMMA-g-HA) was found to be only slightly reduced after 30 min of exposure to the bacterial suspension and is not statistically significant pristine PMMA. Even though this surface was successful in preventing mammalian cell adhesion, the prevention of bacterial adhesion did not occur. XPS and ToF-SIMS analysis was carried out for PMMA-g-HA surfaces exposed to just the LB broth

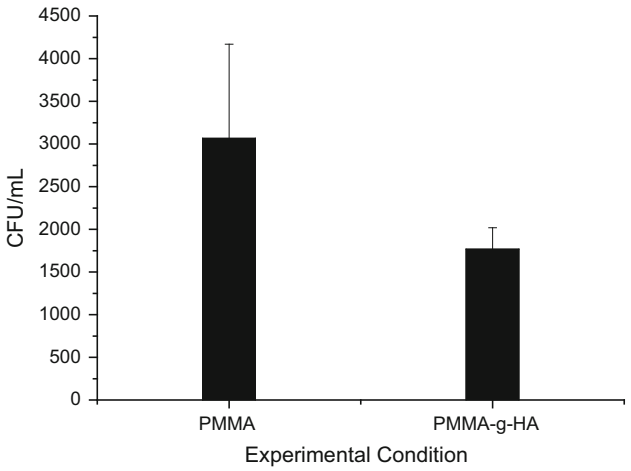

Fig. 9 The number of CFU/mL of *S. aurues* adhering on the variously modified PMMA and PMMA-g-HA surfaces after 30 min of incubation

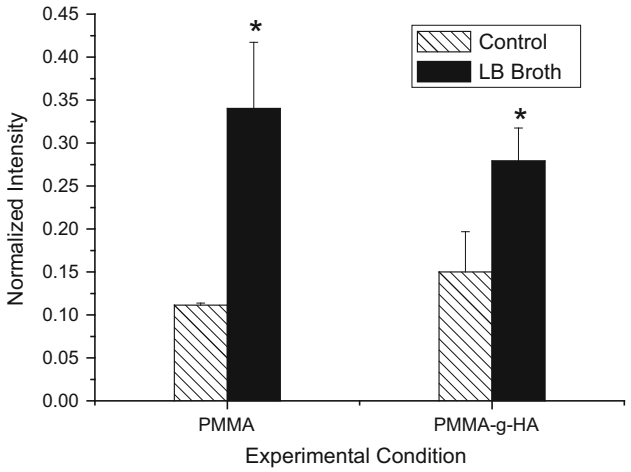

Fig. 10 ToF-SIMS data for PMMA and PMMA-g-HA surfaces before and after adsorption experiments with the LB growth medium. The sum of the intensities of the amino acid fragment ions, $C_2H_5S^+$ (*m/z* 61), $C_3H_4NO^+$ (*m/z* 70), $C_3H_8NO^+$ (*m/z* 74), and $C_4H_6NO^+$ (*m/z* 84), is normalised against the sum of the three characteristic HA fragment ions, m/z 30, 41 and 58 amu corresponding to CH_4N^+, $C_2H_3N^+$ and $C_3H_8N^+$. * indicates statistically significant differences with $P < 0.05$ between surfaces prior to LB exposure and after adsorption

without the bacterial cells. The resulting spectra indicated that XPS analysis was not sensitive enough to determine if components of the broth adhered to the PMMA-g-HA surface. However, as indicated in Fig. 10, ToF-SIMS spectra showed that amino acid fragments were present after incubation. Previously reported data from ToF-SIMS analysis of a bulk film of broth deposited onto a silicon wafer show positive ions originating from the fragmentation of methionine ($C_2H_5S^+$: *m/z* 61), asparagine and proline ($C_3H_4NO^+$: *m/z* 70), $C_3H_8NO^+$ (*m/z* 74), and threonine ($C_4H_6NO^+$: *m/z* 84) [41]. The ToF-SIMS spectrum obtained here shows the peaks at m/z 61, 70, 74 and 84 the intensity of which is indicative of adsorption of amino acids or peptide fragments from the broth onto the PMMA-g-HA surface.

4 Discussion

Successful grafting of HA onto PMMA was achieved using DBD plasma activation of the polymer surface followed by the immobilisation of an APTMS linker layer. ToF-SIMS imaging has shown that the grafting process produces a coherent HA coating on the PMMA substrate that is capable of preventing the adhesion and thereby the proliferation of hCEC. The mean dehydrated thickness of the coatings is less than the XPS sampling depth (~5–10 nm), but within the ToF-SIMS depth of analysis (2–3 nm), which is indicative of an immobilised monolayer of dehydrated polysaccharide coils. Based on these data and previous work, the HA macromolecules are assumed to comprise chains that are randomly attached at several pinning points [21]. These chains have chain ends that can extend into aqueous solution owing to their good solvation in water. It is therefore proposed that it is then the efficient steric-entropic barrier created by the chain ends of the immobilised HA structure that repel hCEC adhesion from the PMMA-g-HA surfaces.

General protein adsorption studies using ToF-SIMS analysis of BSA on PMMA-g-HA showed low levels of adsorption of peptide fragments. Even though amino acid residue peaks are clearly visible in the positive ion spectra, the most abundant peak is at m/z 58 corresponding to $C_3H_8N^+$ of the underlying PMMA-g-HA surface. HSA is a heart-shaped helical protein with approximate dimensions of 8 nm × 8 nm × 3 nm based on its reported crystal structure [42]. The structure of BSA is thought to be similar to HSA due to a 76 % amino acid sequence homology [43]. ToF-SIMS has a sampling depth of 2–3 nm which is smaller than the dimensions of the BSA. As the underlying PMMA-g-HA surface contributes to the resulting spectral data, this indicates that BSA is not present as coherent monolayer but rather is more sporadically adsorbed due to defects in the HA layer. The salient point of note here is that even though there is a low level of protein adsorption, the PMMA-g-HA surface is not sufficient to promote the adhesion of hCECs in vitro.

In the case of the bacterial response to the PMMA-g-HA coatings, colonisation data indicate that the HA surface structure does not provide a sufficient steric entropic contribution to overcome the attractive interfacial forces for bacterial cell adhesion. Anchorage dependent mammalian cells adhere to surfaces via an adlayer of protein [44]. Bacterial adhesion can also occur by the same mechanism

and so, in theory, mammalian cell repellent surfaces should be good candidates for the prevention of bacterial adhesion. Bacteria, however, are much more persistent than mammalian cells and so adhesion can occur by various mechanisms including biospecific (protein–protein, carbohydrate–protein) and non-biospecific (hydrophobic or electrostatic) processes [45]. Various reports in the literature have shown that cell repellent surfaces are able to repel bacterial adhesion [46, 47], however, there have also been reports that show the contrary. For example, Kingshott et al. modified stainless steel with PEG which prevented protein adsorption, but not bacterial adhesion [41]. In addition, Whitesides et al. have also demonstrated that mammalian cell adhesion behaviour does not correlate directly to bacterial cell adhesion on self-assembled monolayers [48]. Hence, our results indicate that for the PMMA-g-HA samples produced using plasma assisted process, there is no link between the surface's ability to repel mammalian cells adhesion and the behaviour of bacterial cell adhesion.

Attaining a full understanding of how HA-coated polymer surfaces behave in the biological milieu is challenging. The failure of the coatings created here to be fully effective in preventing *S. aureus* colonisation may be related to an insufficient packing density of the grafted HA. Attili et al. have shown that end-grafted HA in low ionic strength solutions have chains that have become almost fully stretched such that that the effective HA brush thickness decreases by more than fivefold with increasing ionic strength [49]. de Kerchove et al. have shown that the presence of a threshold amount of calcium and magnesium ions plays a major role in bacterial adhesion and biofilm formation on alginate films [50]. Detailed characterisation of the microstructure of the HA grafted film is a complex and is currently underway to determine the parameter necessary for the HA coatings repel bacterial adhesion.

5 Conclusions

PMMA surfaces were successfully modified by exposure to an atmospheric pressure DBD plasma regime. Whereas, the induced changes to the polymer surface chemistry and topography are relative subtle, they are sufficient to provide for the embolisation of an APTMS layer that has pendant amino group functionality. The adlayer conformation of the silane is capable of undergoing carbodiimide chemistry to bind HA to the modified PMMA. The presence of the HA on the PMMA-g-APTMS surface has been confirmed by XPS, ToF-SIMS and AFM.

The PMMA-g-HA surface has been found to produce only a significant reduction in the amount of BSA adsorbed from solution as compared to that for the PMMA control. However, the fact that hCECs do not adhere or proliferate on the HA modified surface indicates that it can repel the formation of a coherent protein adlayer. The presence of protein, albeit in a non-optimal conformation does however allow for bacterial adhesion to occur. This latter effect confirms that the conditions needed for cell and bacterial adhesion can differ significantly at the molecular level and that this needs to be taken into account when designing medical devices.

Acknowledgments The authors wish to thank Professor Rachel Williams, University of Liverpool for the provision of the corneal epithelial cell line (Dr. K. Araki-Sasaki's Kagoshima, Japan). Financial support from the Department for Employment and Learning, Northern Ireland under the Cross Border Research and Development Funding Programme - Strengthening the All-island Research Base for Functional Biomaterials (DEL-UU-05) is acknowledged.

References

1. Hicks CR, Fitton JH, Chirila TV, Crawford GJ, Constable IJ. Keratoprostheses: advancing toward a true artificial cornea. Surv Ophthalmol. 1997;42(2):175–89.
2. Khan B, Dudenhoefer EJ, Dohlman CH. Keratoprosthesis: an update. Curr Opin Ophthalmol. 2001;12(4):282–7.
3. Griffith M, Hakim M, Shimmura S, Watsky MA, Li F, Carlsson D, et al. Artificial human corneas: scaffolds for transplantation and host regeneration. Cornea. 2002;21:S54–61.
4. Cardona H. Keratoprosthesis: acrylic optical cylinder with supporting intralamellar plate. Am J Ophthalmol. 1962;54(2):284–94.
5. Lloyd AW, Faragher RG, Denyer SP. Ocular biomaterials and implants. Biomaterials. 2001;22(8):769–85.
6. D'Sa RA, Burke GA, Meenan BJ. Protein adhesion and cell response on atmospheric pressure dielectric barrier discharge-modified polymer surfaces. Acta Biomater. 2010;6(7):2609–20.
7. Brash JL. Exploiting the current paradigm of blood–material interactions for the rational design of blood-compatible materials. J Biomater Sci Polym Ed. 2000;11(11):1135–46.
8. Anderson JM, Rodriguez A, Chang DT. Foreign body reaction to biomaterials. Semin Immunol. 2008;20:86–100.
9. Anderson JM. Biological responses to materials. Ann Rev Mater Res. 2001;31(1):81–110.
10. D'Sa RA, Burke GA, Meenan BJ. Lens epithelial cell response to atmospheric pressure plasma modified poly (methylmethacrylate) surfaces. J Mater Sci. 2010;21(5):1703–12.
11. Hosseini S, Ibrahim F, Djordjevic I, Koole LH. Recent advances in surface functionalization techniques on polymethacrylate materials for optical biosensor applications. Analyst. 2014; 139(12):2933–43.
12. D'Sa RA, Raj J, McMahon M, McDowell DA, Burke GA, Meenan BJ. Atmospheric pressure plasma induced grafting of poly (ethylene glycol) onto silicone elastomers for controlling biological response. J Colloid Interface Sci. 2012;375(1):193–202.
13. Laurent TC, Fraser JR. Hyaluronan. FASEB J. 1992;6(7): 2397–404.
14. Fraser JR, Laurent TC. Hyaluronan. In: Comper WD, editor. Extracellular matrix, vol. 2., Molecular Components and Interactions. Amsterdam: Harwood Academic Publishers; 1996. p. 141–99.
15. Laurent TC. Structure of hyaluronic acid. In: Balasz E, editor. Chemistry and molecular biology of the intracellular matrix. London: Academic Press; 1970. p. 709–32.

16. Toole BP. Proteoglycans and hyaluronan in morphogenesis and differentiation. In: Hay ED, editor. Cell biology of the extracellular matrix. New York: Plenum Press; 1991. p. 305.
17. White CJ, Thomas CR, Byrne ME. Bringing comfort to the masses: a novel evaluation of comfort agent solution properties. Contact Lens Anterior Eye. 2014;37(2):81–91.
18. López-García JS, García-Lozano I, Rivas L, Ramírez N, Raposo R, Méndez MT. Autologous serum eye drops diluted with sodium hyaluronate: clinical and experimental comparative study. Acta Ophthalmol. 2014;92(1):e22–9.
19. Suri S, Banerjee R. In vitro evaluation of in situ gels as short term vitreous substitutes. J Biomed Mater Res A. 2006;79(3):650–64.
20. Alauzun JG, Young S, D'Souza R, Liu L, Brook MA, Sheardown HD. Biocompatible, hyaluronic acid modified silicone elastomers. Biomaterials. 2010;31(13):3471–8.
21. D'Sa RA, Dickinson PJ, Raj J, Pierscionek BK, Meenan BJ. Inhibition of lens epithelial cell growth via immobilisation of hyaluronic acid on atmospheric pressure plasma modified polystyrene. Soft Matter. 2011;7(2):608–17.
22. Singh A, Corvelli M, Unterman SA, Wepasnick KA, McDonnell P, Elisseeff JH. Enhanced lubrication on tissue and biomaterial surfaces through peptide-mediated binding of hyaluronic acid. Nat Mat. 2014;13:988–95.
23. Ombelli M, Costello L, Postle C, Anantharaman V, Meng QC, Composto RJ, et al. Competitive protein adsorption on polysaccharide and hyaluronate modified surfaces. Biofouling. 2011;27(5):505–18.
24. Yue Z, Liu X, Molino PJ, Wallace GG. Bio-functionalisation of polydimethylsiloxane with hyaluronic acid and hyaluronic acid–collagen conjugate for neural interfacing. Biomaterials. 2011;32(21):4714–24.
25. D'Sa RA, Meenan BJ. Chemical grafting of poly (ethylene glycol) methyl ether methacrylate onto polymer surfaces by atmospheric pressure plasma processing. Langmuir. 2009;26(3):1894–903.
26. Liu C, Cui N, Brown NM, Meenan BJ. Effects of DBD plasma operating parameters on the polymer surface modification. Surf Coat Technol. 2004;185(2):311–20.
27. Liu C, Brown NM, Meenan BJ. Dielectric barrier discharge (DBD) processing of PMMA surface: optimization of operational parameters. Surf Coat Technol. 2006;201(6):2341–50.
28. Cui N-Y, Upadhyay DJ, Anderson CA, Meenan BJ, Brown NM. Surface oxidation of a Melinex 800 PET polymer material modified by an atmospheric dielectric barrier discharge studied using X-ray photoelectron spectroscopy and contact angle measurement. Appl Surf Sci. 2007;253(8):3865–71.
29. Liu C, Brown NM, Meenan BJ. Uniformity analysis of dielectric barrier discharge (DBD) processed polyethylene terephthalate (PET) surface. Appl Surf Sci. 2006;252(6):2297–310.
30. Chastain J. Handbook of X-ray photoelectron spectroscopy. Minnesota: Perkin-Elmer Corporation; 1992.
31. Araki-Sasaki K, Ohashi Y, Sasabe T, Hayashi K, Watanabe H, Tano Y, et al. An SV40-immortalized human corneal epithelial cell line and its characterization. IOVS. 1995;36(3):614–21.
32. Tang H, Cao T, Wang A, Liang X, Salley SO, McAllister JP, et al. Effect of surface modification of siliconeon Staphylococcus epidermidis adhesion and colonization. J Biomed Mater Res A. 2007;80(4):885–94.
33. Zhang L, Chen Y, Dong T. Studies on the adhesion between polytetra-fluoroethylene film and silanized glass foil. Surf Interface Anal. 2004;36(4):311–6.
34. Allen GC, Sorbello F, Altavilla C, Castorina A, Ciliberto E. Macro-, micro-and nano-investigations on 3-aminopropyltrimethoxysilane self-assembly-monolayers. Thin Solid Films. 2005;483(1):306–11.
35. Bierbaum K, Kinzler M, Wöll C, Grunze M, Hähner G, Heid S, et al. A near edge X-ray absorption fine structure spectroscopy and X-ray photoelectron spectroscopy study of the film properties of self-assembled monolayers of organosilanes on oxidized Si (100). Langmuir. 1995;11(2):512–8.
36. Harder P, Bierbaum K, Woell C, Grunze M, Heid S, Effenberger F. Induced orientational order in long alkyl chain aminosilane molecules by preadsorbed octadecyltrichlorosilane on hydroxylated Si (100). Langmuir. 1997;13(3):445–54.
37. Magalhaes JL, Moreira LM, Rodrigues-Filho UP, Giz MJ, Pereira-da-Silva MA, Landers R, et al. Surface chemistry of the iron tetraazamacrocycle on the aminopropyl-modified surface of oxidized n-Si (100) by AFM and XPS. Surf Interface Anal. 2002;33(4):293–8.
38. Kristensen EM, Nederberg F, Rensmo H, Bowden T, Hilborn J, Siegbahn H. Photoelectron spectroscopy studies of the functionalization of a silicon surface with a phosphorylcholine-terminated polymer grafted onto (3-aminopropyl) trimethoxysilane. Langmuir. 2006;22(23):9651–7.
39. Stile RA, Barber TA, Castner DG, Healy KE. Sequential robust design methodology and X-ray photoelectron spectroscopy to analyze the grafting of hyaluronic acid to glass substrates. J Biomed Mater Res. 2002;61(3):391–8.
40. Pasqui D, Atrei A, Barbucci R. A novel strategy to obtain a hyaluronan monolayer on solid substrates. Biomacromolecules. 2007;8(11):3531–9.
41. Wei J, Ravn DB, Gram L, Kingshott P. Stainless steel modified with poly (ethylene glycol) can prevent protein adsorption but not bacterial adhesion. Colloid Surf B. 2003;32(4):275–91.
42. Sugio S, Kashima A, Mochizuki S, Noda M, Kobayashi K. Crystal structure of human serum albumin at 2.5 Å resolution. Protein Eng. 1999;12(6):439–46.
43. Huang BX, Kim H-Y, Dass C. Probing three-dimensional structure of bovine serum albumin by chemical cross-linking and mass spectrometry. J Am Soc Mass Spectrom. 2004;15(8):1237–47.
44. Chen CS, Mrksich M, Huang S, Whitesides GM, Ingber DE. Geometric control of cell life and death. Science. 1997;276(5317):1425–8.
45. Habash M, Reid G. Microbial biofilms: their development and significance for medical device—related infections. J Clin Pharmacol. 1999;39(9):887–98.
46. Statz AR, Barron AE, Messersmith PB. Protein, cell and bacterial fouling resistance of polypeptoid-modified surfaces: effect of side-chain chemistry. Soft Matter. 2008;4(1):131–9.
47. Chapman RG, Ostuni E, Liang MN, Meluleni G, Kim E, Yan L, et al. Polymeric thin films that resist the adsorption of proteins and the adhesion of bacteria. Langmuir. 2001;17(4):1225–33.
48. Ostuni E, Chapman RG, Liang MN, Meluleni G, Pier G, Ingber DE, et al. Self-assembled monolayers that resist the adsorption of proteins and the adhesion of bacterial and mammalian cells. Langmuir. 2001;17(20):6336–43.
49. Attili S, Borisov OV, Richter RP. Films of end-grafted hyaluronan are a prototype of a brush of a strongly charged, semiflexible polyelectrolyte with intrinsic excluded volume. Biomacromolecules. 2012;13(5):1466–77.
50. De Kerchove AJ, Elimelech M. Calcium and magnesium cations enhance the adhesion of motile and nonmotile *Pseudomonas aeruginosa* on alginate films. Langmuir. 2008;24(7):3392–9.